

A&A manuscript no.
(will be inserted by hand later)

Your thesaurus codes are:
03 (12.03.3; 12.12.1; 11.03.1; 11.04.1)

ASTRONOMY
AND
ASTROPHYSICS

Spectroscopic confirmation of clusters from the ESO imaging survey [★]

M. Ramella¹, A. Biviano¹, W. Boschin¹, S. Bardelli², M. Scodeggio^{3,4}, S. Borgani^{5,6}, C. Benoist^{4,7}, L. da Costa⁴, M. Girardi⁸, M. Nonino^{1,4}, and L.F. Olsen⁹

¹ Osservatorio Astronomico di Trieste, via G.B. Tiepolo 11, I-34131 Trieste, Italy

² Osservatorio Astronomico di Bologna, via Ranzani 1, I-40127 Bologna, Italy

³ Istituto di Fisica Cosmica “G. Occhialini”, via Bassini 15, I-20133 Milano, Italy

⁴ European Southern Observatory, Karl-Schwarzschild-Strasse 2, D-85748 Garching bei München, Germany

⁵ INFN, Sezione di Trieste, c/o Dipartimento di Astronomia, Università degli Studi di Trieste, via G.B. Tiepolo 11, I-34131 Trieste, Italy

⁶ INFN, Sezione di Perugia, c/o Dipartimento di Fisica dell’Università, via A. Pascoli, I-06123, Perugia, Italy

⁷ DAEC, Observatoire de Paris-Meudon, 5 Pl. J. Janssen, F-92195 Meudon Cedex, France

⁸ Dipartimento di Astronomia, Università degli Studi di Trieste, via G.B. Tiepolo 11, I-34131 Trieste, Italy

⁹ Copenhagen University Observatory, Juliane Maries Vej 30, DK-2100, Copenhagen, Denmark

Received March 23, 2000; accepted May 9, 2000

Abstract. We measure redshifts for 67 galaxies in the field of six cluster candidates from the ESO Imaging Survey (EIS). The cluster candidates are selected in the EIS patches C and D among those with estimated mean redshifts $0.5 \leq z \leq 0.7$. The observations were made with EFOSC2 at the 3.6m ESO telescope.

In the six candidate cluster fields, we identify 19 possible sets of 2 to 7 galaxies in redshift space. In order to establish which of the 19 sets are likely to correspond to real dense systems we compare our counts with those expected from a uniform distribution of galaxies with given luminosity function. In order to take into account the effect of the Large Scale Structure, we modulate the probability computed from the luminosity function with random samplings of the Canada-France Redshift Survey.

We find that four out of six candidate EIS clusters are likely to correspond to real systems in redshift space ($> 95\%$ confidence level). Two of these systems have mean redshift in agreement with the redshift estimate given by the matched filter algorithm ($\Delta z = \pm 0.1$). The other two systems have significantly lower redshifts.

We discuss the implications of our results in the context of our ongoing research projects aimed at defining high-redshift optically-selected cluster samples.

Key words: Cosmology: observations – large-scale structure of Universe – Galaxies: clusters: general – Galaxies: distances and redshifts

1. Introduction

Clusters of galaxies are the largest virialized structures observed in the Universe. Since they arise from exceptionally high peaks of the primordial fluctuation density field, their properties are highly sensitive to the nature of such cosmic fluctuations. Therefore, the mass function of both local (e.g. White et al. 1993; Girardi et al. 1998) and distant clusters (e.g. Oukbir & Blanchard 1992; Carlberg et al. 1997; Eke et al. 1998; Borgani et al. 1999) is a powerful tool to constrain cosmological models for the formation and evolution of cosmic structures. Moreover, clusters are useful laboratories for testing models of galaxy evolution. While early-type galaxies only show evidence for passive evolution (e.g. Stanford et al. 1998), the fraction of blue galaxies increases significantly with redshift (Butcher & Oemler 1978), at least up to $z \sim 0.5$, and the fraction of S0’s decreases (Dressler et al. 1999). It is therefore essential to have reliable cluster catalogues over the largest possible redshift range.

Most distant clusters, at $z \geq 0.5$, have so far been identified through optical follow-ups of X-ray selected clusters (see, e.g. Gioia et al. 1990 and Rosati et al. 2000 for a recent review), or by looking at the environment of high-redshift radio galaxies (e.g. Smail & Dickinson 1995; Deltorn et al. 1997).

In the optical, clusters at $z \simeq 0.5$ and beyond started to be classified in the 80’s (Gunn et al. 1986). In the 90’s a large catalogue of objectively selected distant clusters, identified in the optical, became available (Postman et al. 1996). These last clusters are identified using a matched-filter algorithm using both positional and photometric data. In brief, this algorithm filters a galaxy catalogue to remove fluctuations in the projected distribution

Send offprint requests to: M. Ramella, ramella@oat.ts.astro.it

[★] Based on observations collected at the European Southern Observatory (La Silla, Chile), Proposal ID: 62.O-0601

of galaxies that are not likely to be galaxy clusters. For this purpose, the filter is built around parametrizations of the spatial distribution and luminosity function of cluster galaxies. This algorithm also provides an estimate of the redshift for each candidate cluster (hereafter we refer to the matched-filter estimated redshift as z_{mf}). Currently, $\simeq 30$ PDCS clusters have been confirmed spectroscopically, most of them at $z < 0.5$ (Holden et al. 1999a, 1999b; Oke et al. 1998).

Recently, Olsen et al. (1999a, 1999b) and Scodreggio et al. (1999) have presented a catalogue of 302 cluster candidates from the *I*-band images of the ESO Imaging Survey (EIS, see Renzini & da Costa 1997). Clusters are identified in two dimensions (hereafter, 2-d) using the matched filter algorithm of Postman et al. (1996; see Olsen et al. 1999a). The estimated redshifts for EIS clusters span the range $0.2 \leq z_{mf} \leq 1.3$, with a median redshift $z_{mf} = 0.5$.

Several EIS cluster candidates have been confirmed so far, most at $z < 0.5$, either from the existence of the red sequence of cluster ellipticals/S0's in colour-magnitude diagrams (Olsen et al. 1999b), or from a combination of photometric and spectroscopic data (da Costa et al. 1999).

The EIS cluster catalogue is the largest optically selected cluster sample currently available in the Southern Hemisphere to this depth. This catalogue constitutes an obvious reference for follow-up observations at the ESO VLT aimed at determining the structure and dynamics of distant clusters, as well as the spectroscopic properties of their member galaxies. Unfortunately, little is currently known on the performance of the matched filter algorithm in detecting real clusters at $z \geq 0.5$. As we already pointed out, most confirmed PDCS and EIS clusters have redshifts $z < 0.5$. Therefore, to point blindly at EIS cluster candidates would make for an inefficient use of VLT time, because we expect several of these candidate clusters not to be real, in particular at $z_{mf} \geq 0.5$.

The aim of our investigation is twofold: we want to confirm as many EIS clusters as possible, in order to build a reliable sample of distant clusters with well determined redshift, and, at the same time, evaluate the performance of the matched filter algorithm in the detection of high-redshift clusters. In order to achieve this purpose, we use two independent methods: (1) multi-object spectroscopic observations of EIS cluster candidates in the redshift range $0.5 \leq z_{mf} \leq 0.7$, and (2) the detection of the colour-magnitude sequences traced by early-type galaxies through multi-colour optical and near-IR photometry of the most distant EIS cluster candidates (Scodreggio et al., in preparation).

In this paper we report the first results of the spectroscopic investigations of 6 EIS clusters. We are able to confirm the existence of significant concentrations in redshift space in correspondence of four of the six EIS fields targeted. For two of these confirmed clusters, the spectroscopic mean redshift agrees with the matched-filter estimate to within $\Delta z = \pm 0.1$.

In Sect. 2 we describe our spectroscopic observations, data reduction, and give the new galaxy redshifts. In Sect. 3 we analyse the data, and define sets of galaxies in redshift space. We also discuss the concordance of the mean redshifts of these sets with the matched-filter estimates of the cluster mean redshifts. We then make a likelihood analysis of the reality of the galaxy sets, and flag four of them as reliable at $> 95\%$ confidence level (Sect. 4). Finally, we discuss our results and give our conclusions in Sect. 5.

We use $H_0 = h_{75} 75 \text{ km s}^{-1} \text{ Mpc}^{-1}$, $\Omega_0 = 0.2$ and $\Omega_\Lambda = 0$ throughout this paper, unless otherwise stated.

2. Observations and data reduction

We select our targets among the candidate EIS clusters in patches C and D, with estimated redshift $0.5 \leq z_{mf} \leq 0.7$ (Scodreggio et al. 1999). We do not apply any additional criterion for the selection of our cluster candidates. The size of our sample is one tenth of the total of 36+28 EIS clusters in patches C and D within the above-mentioned redshift range.

Our targets are listed in Table 1. In Column (1) we list the cluster candidate identification name, in Column (2) and (3) the right ascension and declination (J2000), in Column (4) the cluster richness (see Olsen et al. 1999a), and in Column (5) the matched-filter redshift estimate, z_{mf} (see Scodreggio et al. 1999). In Column (6) we list the number of galaxies targeted for multi-slit spectroscopy in each cluster field, and in Column (7) the number of successful redshift estimates.

The observations were carried out at the 3.6 m ESO telescope at La Silla, Chile, during two nights in February 1999. The weather conditions were good, with seeing slightly above $1''$, in partial moonlight. With a total useful observing time of 16 hours over the two nights, we were able to obtain 3×45 min exposures for each cluster.

We observed with EFOSC2 in Multi-Object Spectroscopy (MOS) mode. EFOSC2 was equipped with a Loral CCD of 2048×2048 with $15 \mu\text{m}$ pixels, allowing for an unvignetted field-of-view of $3.8' \times 5.5'$. We used Grism # 1, giving a spectral range 3185–10940 Å, and a dispersion of 6.3 Å/pixel . On the MOS masks our slits were $1.2''$ wide.

We obtained spectra for 102 objects in the magnitude range $17.0 \leq m_I \leq 21.3$, where m_I is the apparent magnitude in the I_c band (Nonino et al. 1999). In Fig. 1–6 we show I_c -band images of the six EIS candidate clusters. Small circles mark galaxies with redshift, large circles mark galaxies belonging to significant overdensities in redshift space (see Sect. 4).

We reduce the data with standard IRAF¹ packages. We determine redshifts using the task XCSAO that implements the cross-correlation technique of Tonry & Davis

¹ IRAF is distributed by the National Optical Astronomy Observatories, which is operated by AURA Inc. under contract with NSF

Table 1. Cluster candidates selected for observation

Id.	α_{J2000}	δ_{J2000}	Λ_{cl}	z_{mf}	n_{slits}	n_z
EIS0533-2353	05:33:36.5	-23:53:52.9	72.0	0.7	16	12
EIS0540-2418	05:40:08.5	-24:18:19.3	83.8	0.6	20	14
EIS0950-2154	09:50:47.9	-21:54:38.3	62.4	0.5	18	11
EIS0951-2047	09:51:32.5	-20:47:08.3	65.1	0.5	15	11
EIS0955-2113	09:55:32.3	-21:13:55.3	68.2	0.6	17	7
EIS0956-2009	09:56:28.6	-20:09:27.4	58.2	0.5	16	13

See eis_efosc2.f1.gif

Fig. 1. An I_c -band image of the EIS0533-2353 cluster candidate. The circles indicate those galaxies for which we obtained redshifts. The field is $6.4' \times 4.3'$, centered at $\alpha = 05:33:36.5$, $\delta = -23:53:53$ (J2000). North is up, East is to the left.

(1979). We use several real and synthetic templates for the cross-correlation. We use emission lines, where present in the spectrum of the object, to determine the redshift with the task EMSAO. We examine visually all spectra, by overplotting the positions of the major spectral features redshifted at the redshift(s) determined by the automatic techniques described above. We employ particular care in flagging those features that could be contaminated by night-sky lines.

In total, we determine 67 galaxy redshifts, from a minimum of $z = 0.09$ to a maximum of $z = 0.79$, with an av-

erage $\bar{z} = 0.380$. One of our objects turns out to be a QSO at $z = 3.2$. We do not consider this object in our analysis. An internal estimate of the typical redshift uncertainty is $\delta z \sim 0.001$. The success-rate is magnitude-dependent, as can be seen in Fig. 7: it is 85 % for $m_I \leq 19.5$ and decreases to 57 % for fainter galaxies.

We list in Table 2 the galaxies with measured redshift. In Column (1) we list the name of the EIS candidate cluster field, in Column (2) a galaxy identification number, in Column (3) and (4) the (J2000) right ascension and the declination of the galaxy, in Column (5) the I_c magnitude,

See eis_efosc2.f2.gif

Fig. 2. Same as Fig. 1, for the EIS0540-2418 cluster candidate. The field is centered at $\alpha = 05:40:08.5$, $\delta = -24:18:19$ (J2000).

in Column (6) the redshift, and in Column (7) the galaxy set to which the galaxy is assigned. These galaxy sets are defined in Sect. 3 and listed in Table 3.

3. The definition of the galaxy systems in redshift space

Since the six cluster candidates are drawn from the EIS cluster catalogue, they obviously correspond to significant density enhancements in projection. Here we search for systems of galaxy redshifts that could be associated to the 2-d over-densities. In this way we assign a spectroscopic redshift to 4 of our cluster candidates. We also evaluate the probability that these systems correspond to a genuine three-dimensional cluster.

Olsen et al. (1999a) search for clusters in projection assuming a 2-d radial density profile with a cutoff radius $r_{co} = 1.33 h_{75}^{-1}$ Mpc. This size is well fitted to the EFOSC2 field-of-view, corresponding to $1.9 \times 1.3 h_{75}^{-2}$ Mpc², at $z \sim 0.6$ (the average estimated redshift of our candi-

date clusters). Therefore, we search for cluster members in redshift-space within the whole EFOSC2 field.

Several refined algorithms for the definition of systems of galaxies in redshift space can be found in the literature (e.g. Katgert et al. 1996; Pisani 1993). However, with only a dozen galaxy redshifts per field, these sophisticated algorithms can not be applied. We choose to identify galaxy systems using a physical criterion based on the well established properties of nearby clusters of galaxies.

Within each EFOSC2 field, we identify any set of two or more galaxies contained within a given redshift range, Δz . In order to define Δz , we note that Abell-like clusters of galaxies have mean velocity dispersions $\sigma_v \simeq 750 \text{ km s}^{-1}$ (Girardi et al. 1993). Since the line-of-sight velocity distributions of clusters are approximately gaussian in shape (Girardi et al. 1993), $> 99 \%$ of the cluster members have a velocity within $\pm 3\sigma_v$. As a consequence, galaxies in a given cluster should be located within a redshift range $\Delta z \leq 0.015 \times (1 + z)$, taking into account the cosmological factor (Danese et al. 1980).

Table 2. Galaxies in the six EIS cluster fields

Field id.	Galaxy id.	α_{J2000}	δ_{J2000}	m_I	z	galaxy set
EIS0533-2353	401117	05:33:31.16	-23:51:52.9	19.40	0.311	1b
	391647	05:33:31.56	-23:53:27.6	19.04	0.332	1c
	395828	05:33:32.05	-23:52:46.9	20.25	0.335	1c
	394374	05:33:33.78	-23:52:55.3	19.72	3.2	
	391769	05:33:33.86	-23:53:19.3	20.25	0.274	1a
	391224	05:33:34.77	-23:53:27.2	20.06	0.497	1d
	391895	05:33:35.18	-23:53:29.6	18.46	0.305	1b
	387448	05:33:35.26	-23:54:00.6	20.52	0.509	1d
	391850	05:33:38.24	-23:53:19.6	20.73	0.206	
	386188	05:33:38.58	-23:54:10.1	20.97	0.176	
	391395	05:33:42.00	-23:53:26.4	20.70	0.42	
	378902	05:33:42.75	-23:55:21.1	19.19	0.277	1a
EIS0540-2418	211948	05:40:00.44	-24:19:11.3	19.75	0.528	2c
	214076	05:40:01.47	-24:18:53.7	19.57	0.476	2b
	215860	05:40:05.15	-24:18:27.4	21.18	0.467	2b
	217648	05:40:05.42	-24:18:15.0	20.14	0.603	
	219687	05:40:06.33	-24:17:51.4	21.09	0.790	
	217861	05:40:08.82	-24:18:18.6	18.59	0.534	2c
	228555	05:40:09.28	-24:16:37.8	19.93	0.289	
	216666	05:40:12.93	-24:18:35.8	18.72	0.437	2a
	231275	05:40:12.95	-24:16:27.5	19.94	0.087	
	220131	05:40:13.66	-24:18:00.9	20.18	0.698	2d
	220959	05:40:14.98	-24:17:40.9	20.80	0.710	2d
	222317	05:40:15.45	-24:17:30.4	19.77	0.442	2a
	225021	05:40:16.22	-24:17:10.0	20.37	0.519	2c
	223115	05:40:18.12	-24:17:23.3	20.59	0.696	2d
EIS0950-2154	56524	09:50:41.48	-21:53:58.6	19.50	0.215	3b
	51381	09:50:44.84	-21:54:44.2	19.35	0.285	
	44805	09:50:45.40	-21:55:48.3	19.25	0.126	3a
	53238	09:50:47.12	-21:54:22.6	19.86	0.214	3b
	53078	09:50:47.67	-21:54:33.1	19.08	0.486	
	50696	09:50:49.42	-21:54:42.5	20.27	0.456	
	46272	09:50:51.12	-21:55:30.1	17.39	0.129	3a
	45102	09:50:52.24	-21:55:39.2	18.64	0.240	3c
	45447	09:50:52.83	-21:55:32.3	19.00	0.129	3a
	53713	09:50:55.24	-21:54:16.2	20.45	0.622	
	35640	09:50:56.39	-21:56:54.7	19.59	0.242	3c
EIS0951-2047	504012	09:51:23.60	-20:47:30.4	18.46	0.281	
	494234	09:51:24.75	-20:48:33.3	19.09	0.241	4c
	512064	09:51:30.08	-20:46:09.6	19.39	0.234	4c
	505407	09:51:30.46	-20:47:16.6	19.14	0.215	4b
	509165	09:51:30.52	-20:46:35.4	18.76	0.238	4c
	518715	09:51:30.68	-20:45:02.8	18.95	0.187	4a
	489725	09:51:30.81	-20:48:47.1	18.72	0.182	4a
	510378	09:51:31.01	-20:46:18.4	20.43	0.486	
	507808	09:51:31.34	-20:46:41.6	19.61	0.236	4c
	506364	09:51:31.45	-20:46:54.1	17.05	0.236	4c
	519886	09:51:32.71	-20:44:44.2	20.19	0.214	4b
EIS0955-2113	325426	09:55:24.52	-21:14:20.6	19.96	0.341	5a
	326951	09:55:25.97	-21:13:59.7	18.81	0.331	5a
	328968	09:55:31.58	-21:13:48.8	19.46	0.673	5b
	328298	09:55:32.46	-21:13:51.9	19.95	0.656	5b
	329220	09:55:33.70	-21:13:49.2	19.93	0.674	5b
	323973	09:55:34.45	-21:14:30.2	19.56	0.375	
	325779	09:55:40.01	-21:14:10.2	20.09	0.279	

See eis_efosc2.f3.gif

Fig. 3. Same as Fig. 1, for the EIS0950-2154 cluster candidate. Large circles indicate galaxies identified as members of a significant overdensity in redshift space. The field is centered at $\alpha = 09:50:48.6$, $\delta = -21:55:15$ (J2000).

Table 2. Continued.

Field id.	Galaxy id.	α_{J2000}	δ_{J2000}	m_I	z	galaxy set
EIS0956-2009	746450	09:56:20.17	-20:09:35.9	20.73	0.349	6a
	748248	09:56:22.38	-20:09:33.8	19.88	0.443	6c
	751377	09:56:24.32	-20:09:09.6	19.00	0.447	6c
	749243	09:56:25.24	-20:09:14.7	20.55	0.451	6c
	753860	09:56:26.21	-20:08:32.8	19.76	0.443	6c
	745962	09:56:26.33	-20:09:41.4	20.26	0.362	6a
	748889	09:56:27.66	-20:09:03.0	18.26	0.363	6a
	751960	09:56:28.11	-20:09:01.7	19.36	0.445	6c
	751382	09:56:28.96	-20:09:05.2	18.80	0.444	6c
	753734	09:56:29.04	-20:08:40.0	19.63	0.369	6a
	752280	09:56:31.79	-20:08:53.9	19.38	0.402	6b
	750180	09:56:34.08	-20:08:46.0	19.49	0.392	6b
	754800	09:56:35.18	-20:08:28.0	19.00	0.441	6c

We list in Table 3 the sets of galaxies we identify in redshift space. In Column (1) we list the EIS cluster field identification, in Column (2) the galaxy set identification, in Column (3) the number of galaxies in the set, in Column (4) the median redshift of the set, in Column (5) the total

redshift range covered by the galaxies within the galaxy set. In Column (6) we list the probability of the galaxy set to correspond to a significant overdensity in redshift space, as estimated from resamplings of the Canada-France Redshift Survey data-base (CFRS; Lilly et al. 1995; Le Fèvre

See eis_efosc2.f4.gif

Fig. 4. Same as Fig. 1, for the EIS0951-2047 cluster candidate. Large circles indicate galaxies identified as members of a significant overdensity in redshift space. The field is centered at $\alpha = 09:51:31.8$, $\delta = -20:46:57$ (J2000).

et al. 1995; Hammer et al. 1995; Crampton et al. 1995) – see Sect. 4. The real systems (probability ≥ 0.95) are flagged in Column (7).

In total we identify 19 galaxy sets along the line-of-sight of six EIS candidate clusters. It is interesting to detail the comparison of the estimated mean redshifts, z_{mf} 's, of these clusters (see Table 1), to the spectroscopic redshifts of the 19 sets (see Table 3). In this comparison, we take into account the uncertainties in the mean redshifts of the galaxy sets, and note that the matched-filter redshift estimates are at most accurate to within $\Delta z = \pm 0.05$.

In the case of the candidate clusters EIS0533-2353, EIS0950-2154, and EIS0951-2047, we do not find any galaxy set close to the estimated cluster redshifts. According to the matched-filter algorithm, these three clusters are located at a higher redshift than any of the galaxy sets found in their fields. In each of the fields of EIS0955-2113 and of EIS0956-2009, there is one set of galaxies with mean redshift close to the estimated redshift ($\bar{z} = 0.673$ vs. $z_{mf} = 0.6$, and $\bar{z} = 0.445$ vs. $z_{mf} = 0.5$, respectively). Finally, in the field of EIS0540-2418, there are two sets of

galaxies with mean redshifts close to the cluster estimated redshift, $z_{mf} = 0.6$.

The detection of galaxy concentrations close to the estimated redshifts of three EIS clusters supports the reliability of the matched-filter redshift estimates.

As far as the failed detections are concerned, EIS0533-2353 may have escaped detection because of its high (estimated) redshift, $z_{mf} = 0.7$ – we may simply have not been observing deep enough. Moreover, the line-of-sight to a single cluster can intercept several different galaxy sets. Katgert et al. (1996) estimate that 10 % of nearby Abell clusters result from the superposition of two almost equally rich systems (and this fraction is probably higher for more distant clusters). The nearest of these systems has the highest chance of being detected. In this context, we note that the low- z set of galaxies, 3a, detected in the field of EIS0950-2154 is somewhat off-centered with respect to the nominal EIS cluster center (see Fig. 3). The same is not true for the sets with $z \sim z_{mf}$ in the fields of EIS0540-2418, EIS0955-2113, and EIS0956-2009. This

See eis_efosc2.f5.gif

Fig. 5. Same as Fig. 1, for the EIS0955-2113 cluster candidate. Large circles are galaxies members of a significant overdensity in redshift space. The field is centered at $\alpha = 09:55:32.1$, $\delta = -21:13:55$ (J2000).

Table 3. Sets of galaxies in the EIS cluster fields

Field id.	galaxy set	N_{gal}	median(z)	Δz	galaxy set probability	$P \geq 95\%$ sets
EIS0533-2353	1a	2	0.276	0.003	0.348	
	1b	2	0.308	0.006	0.210	
	1c	2	0.334	0.003	0.325	
	1d	2	0.503	0.012	0.168	
EIS0540-2418	2a	2	0.440	0.005	0.226	
	2b	2	0.472	0.009	0.125	
	2c	3	0.528	0.015	0.592	
	2d	3	0.698	0.014	0.924	
EIS0950-2154	3a	3	0.129	0.003	0.972	Y
	3b	2	0.214	0.001	0.632	
	3c	2	0.241	0.002	0.500	
EIS0951-2047	4a	2	0.184	0.005	0.478	
	4b	2	0.214	0.001	0.632	
	4c	5	0.236	0.007	0.993	Y
EIS0955-2113	5a	2	0.336	0.010	0.326	
	5b	3	0.673	0.018	0.957	Y
EIS0956-2009	6a	4	0.362	0.020	0.714	
	6b	2	0.397	0.010	0.063	
	6c	7	0.445	0.010	0.997	Y

See eis_efosc2.f6.gif

Fig. 6. Same as Fig. 1, for the EIS0956-2009 cluster candidate. Large circles indicate galaxies identified as members of a significant overdensity in redshift space. The field is centered at $\alpha = 09:56:28.4$, $\delta = -20:09:30$ (J2000).

fact suggests that the set 3a does not correspond to the EIS cluster, but is a foreground group.

Da Costa et al. (2000) suggest that all the six EIS candidate clusters could be real clusters at redshift > 0.5 . Da Costa et al. base their suggestion on the detection of red-sequences of early-type galaxies in the colour-magnitude diagrams. They note that under-sampling of the redshift distribution of galaxies in the cluster fields may explain the lack of spectroscopic detections of some clusters.

where $V(z)$ is the volume element at the redshift z and $f[L(m, z)]$ is the luminosity function (LF hereafter). We take the LF in the I_4 band given by Postman et al. (1996) and convert it to our I_c band, using the Postman et al. transformation procedure. Our reference LF has therefore a Schechter (1976) form with parameters $\alpha = -1.1$ and $M^* = -22.15 + 5 \log h_{75}$. We also assume negligible evolution of the LF out to $z \sim 0.8$ (see Lilly et al. 1995 and Lin et al. 1999). Our LF then depends on z only through the evolution of the stellar populations and the K-correction, that we take from Poggianti (1997).

4. The reality of the galaxy sets

In this Sect. we assign likelihoods to the 19 sets of galaxies which have been identified in the previous Sect. If $s(m)$ is the incompleteness of our redshift sample in the magnitude interval $[m_1, m_2]$ (see Fig. 8), then the redshift distribution reads

$$N(z)dz = \frac{dV(z)}{dz} dz \int_{m_1}^{m_2} f[L(m, z)] s(m) dm, \quad (1)$$

In Fig. 9, we plot $N(z)$, computed according to Eq. 1, along with the observed z -distribution. Based on the estimated $N(z)$, we find that 16 out of 19 sets correspond to significant overdensities in redshift space, with a probability $\geq 95\%$. Since Eq. 1 provides $N(z)$ for a uniform galaxy distribution, these probabilities do not include the effect of large scale clustering (see, e.g., Zaritsky et al. 1997). In order to account for the large scale clustering, and following the approach by Holden et al. (1999a), we

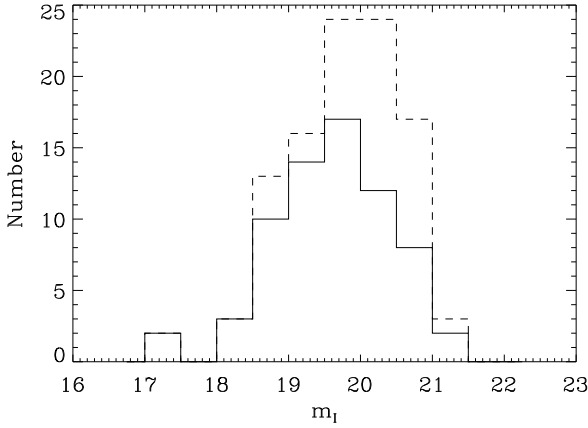


Fig. 7. The I_c -band magnitude distribution of the 102 targets for which we attempted spectroscopy (dashed-line histogram), and of the 67 galaxies (plus a QSO) for which we obtained a redshift (solid-line histogram).

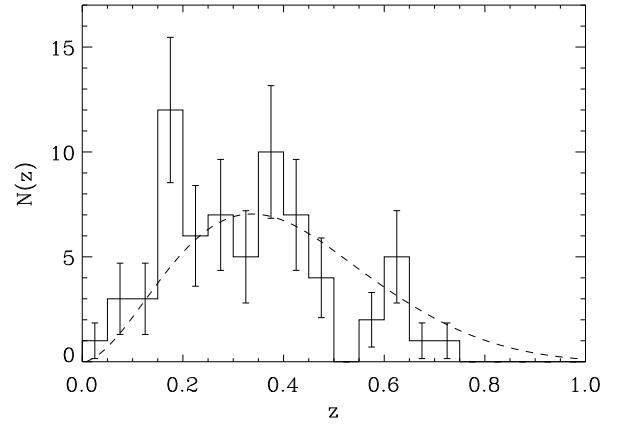


Fig. 9. The redshift distribution function, $N(z)$ (dashed line) and the redshift histogram of the 67 galaxies of our sample in the redshift range $0.0 \leq z \leq 0.8$. $N(z)$ is normalised to the same number of objects, 67.

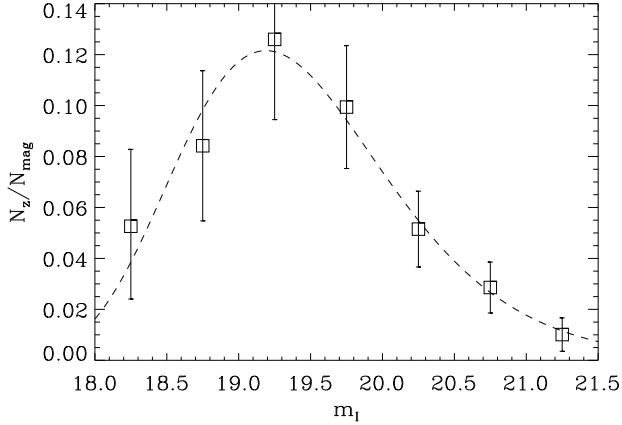


Fig. 8. The function $s(m)$, computed as the ratio between the binned magnitude distributions of galaxies with redshifts, and of galaxies with magnitudes, in the range $17 \leq m_I \leq 21.3$, in the six EIS cluster fields. The dashed line is the best fit to the data with a Schechter function.

modulate $N(z)$ with the redshift distribution derived from the CFRS assuming our selection function, $s(m)$.

We first convert the CFRS I_{AB} magnitudes to the I_c system (see Lilly et al. 1995). We then extract 50000 galaxies from the CFRS, with a bootstrap sampling, adopting the magnitude distribution of our sample (see Fig. 7). A Kolmogorov-Smirnov test shows that the bootstrapped CFRS and our data-set have similar redshift distributions. This is expected since magnitude selection is the main process leading to the inclusion of galaxies in the sample.

We extract random subsamples of 11 galaxies from the bootstrapped CFRS reference sample (11 is the mean number of galaxies with redshift in our EIS cluster fields).

Using the same procedure described in Sect. 3, we identify sets of galaxies within these subsamples, and compute their probabilities relative to the uniform redshift distribution $N(z)$ given by Eq. 1. In this way we construct a distribution of probabilities to detect a real system within a galaxy sample which includes large-scale clustering, but not galaxy clusters. We finally obtain the likelihoods of the 19 observed sets, by comparing their original $N(z)$ -based probabilities to the distribution of probabilities for the random sets. These 19 likelihoods are listed in Table 3.

We find that four of our 19 sets have a likelihood $> 95\%$; all of them have at least three galaxy members. The four sets are flagged in the last column of Table 3. We refer to these four sets as the ‘real systems’ hereafter. As expected, many of the sets with a significant overdensity with respect to the uniform redshift distribution are no longer significant when compared to a redshift distribution which includes the large scale clustering.

Our results are robust against modifications of the adopted LF (we change α by ± 0.2 , and M^* by ± 0.5 mag), and of the galaxy-type for which the evolutionary- and K-corrections are computed. Furthermore, we verify that varying cosmological parameters (h_{75} , Ω_0 and Ω_Λ) within conservative ranges, only induces marginal changes in the system likelihoods. Finally, we also checked that narrowing the Δz range used to define the redshift-sets, from 0.015 to 0.010, hardly modifies the membership and likelihoods of the sets.

5. Discussion and conclusions

We obtain 67 new redshifts for galaxies in six EIS candidate cluster fields. Based on these data, we establish the existence of real systems in redshift space in the direction of four of these candidate clusters. The reality of

the systems is established at > 95 % confidence level, and in two cases, at > 99 %. The redshift overdensities, coupled with the 2-d overdensities detected by the use of the matched-filter algorithm, strongly supports the reality of four of the six examined EIS clusters. These 4 clusters add to the other two spectroscopically confirmed EIS clusters (da Costa et al. 1999).

Two of the four z -systems have a median redshift in good agreement with the matched-filter estimate for the EIS cluster redshift ($|\text{median}(z) - z_{mf}| < 0.1$). The other two have significantly lower redshifts ($\text{median}(z) = 0.129, 0.236$ vs. $z_{mf} = 0.5$).

Taken at face value, these results suggest that, in several cases, the matched-filter algorithm over-estimates the mean cluster redshift by a large amount. However, it is quite possible that in some cases we have not detected the EIS cluster, but a foreground galaxy system projected along the same line-of-sight of the cluster. Similarly, it is difficult to conclude about the reality of the EIS clusters where we do not detect any real redshift system.

In particular, we note that in the field of EIS0540-2418 we have a marginal detection (92 % probability) of the galaxy set 2d at $\text{median}(z) = 0.698$ (see Table 3), in fair agreement with the matched-filter estimate of the cluster redshift, $z_{mf} = 0.6$. We also note that the cluster EIS0533-2353 has $z_{mf} = 0.7$, larger than any of our galaxy sets. This suggests that it could have escaped detection because our observations were not deep enough. In fact, da Costa et al. (2000) suggest that all our six EIS cluster candidates could be real, based on the analysis of the colour-magnitude diagrams for galaxies in the cluster fields.

We conclude that our spectroscopic confirmation rate must be considered as a lower limit. If at least one third of the EIS clusters in the redshift range sampled by our observations are real, there are more than 25 EIS clusters with z_{mf} in the range 0.5–0.7. This sample is large enough for the derivation of the properties of clusters at intermediate to high redshifts.

Optical selection of clusters of galaxies at high redshifts is a necessary complementary approach to X-ray selection. While X-ray selection tends to detect only rich Abell-like clusters, optically selected cluster samples contain a large number of poor clusters. In fact, the space density of PDCS clusters is five times higher than that of rich Abell clusters (Holden et al. 1999a), and very few PDCS clusters are X-ray bright (Holden et al. 1997). Consistently, the velocity dispersions of our two systems with ≥ 5 galaxy redshifts (system 4c, at $\bar{z} = 0.236$ and system 6c, at $\bar{z} = 0.445$, see Table 3) are $\sim 600 \text{ km s}^{-1}$, typical of low-richness clusters ($R \leq 1$, see Girardi et al. 1993).

With the current and near-future ground-based facilities for wide-field optical and near-infrared imaging, we can expect a rapid increase in the samples of optically selected clusters. Currently, our spectroscopic sample only comprises ~ 10 % of all the clusters in the two patches

C and D, and in the (estimated) redshift range 0.5–0.7. We plan to extend our sample in forthcoming observing runs. Confirmed EIS clusters at high redshift will be the natural targets of VLT observations aimed at determining their dynamical properties.

Acknowledgements. We thank Nando Patat for imaging the six EIS fields in preparation for our spectroscopic run.

References

- Borgani S., Girardi M., Carlberg R.G., Yee H.K.C., Ellingson E., 1999, ApJ 527, 561
- Butcher H., Oemler A. Jr., 1978, ApJ 226, 559
- Carlberg R.G., Morris S.L., Yee H.K., Ellingson E., 1997, ApJ 479, L19
- Crampton D., Le Fèvre O., Lilly S.J., Hammer F., 1995, ApJ 455, 88
- da Costa L., Scodreggio M., Olsen L.F., et al., 1999, A&A 343, L29
- da Costa L., Scodreggio M., Olsen L.F., Benoist C., 2000, in “Large Scale Structure in the X-ray Universe”, Eds. Plionis M. & Georgantopoulos I., Santorini, Greece, September 1999 (astro-ph/9912067)
- Danese L., De Zotti G., di Tullio G., 1980, A&A 82, 322
- Deltorn J.-M., Le Fèvre O., Crampton D., Dickinson M., 1997, ApJ 483, L21
- Dressler A., Smail I., Poggianti B.M., et al., 1999, ApJS 122, 51
- Eke V.R., Cole S., Frenk C.S., Henry J.P., 1998, MNRAS 298, 114
- Gioia I.M., Maccacaro T., Schild R.E., Morris S.L., Henry J.P., 1990, ApJS 72, 567
- Girardi M., Biviano A., Giuricin G., Mardirossian F., Mezzetti M., 1993, ApJ 404, 38
- Girardi M., Borgani S., Giuricin G., Mardirossian F., Mezzetti M., 1998, ApJ 506, 45
- Gunn J.E., Hoessel J.G., Oke J.B., 1986, ApJ 306, 30
- Hammer F., Crampton D., Le Fèvre O., Lilly S.J., 1995, ApJ 455, 88
- Holden B.P., Romer A.K., Nichol R.C., Ulmer M.P., 1997, AJ 114, 1701
- Holden B.P., Nichol R.C., Romer A.K., et al., 1999a, AJ 118, 2002
- Holden B.P., Adami C., Nichol R.C., et al., 1999b, AAS Meeting 194
- Katgert P., Mazure A., Perea J., et al., 1996, A&A 310, 8
- Le Fèvre O., Crampton D., Lilly S.J., Hammer F., Tresse L., 1995, ApJ 455, 60
- Lilly S.J., Le Fèvre O., Crampton D., Hammer F., Tresse L., 1995, ApJ 455, 50
- Lin H., Yee H.K.C., Carlberg R.G., et al., 1999, ApJ 518, 533
- Nonino M., Bertin E., da Costa L., et al., 1999, A&AS 137, 51
- Oke J.B., Postman M., Lubin L.M., 1998, AJ 116, 549
- Olsen L.F., Scodreggio M., da Costa L., et al., 1999a, A&A 345, 681
- Olsen L.F., Scodreggio M., da Costa L., et al., 1999b, A&A 345, 363
- Oukbir J., Blamchard A., 1992, A&A 252, L21
- Pisani A., 1993, MNRAS 265, 706
- Poggianti B.M., 1997, A&AS 122, 399

- Postman M., Lubin L.M., Gunn J.E., et al., 1996, AJ 111, 615
- Renzini A., da Costa L.N., 1997, Messenger 87, 23
- Rosati P., Borgani S., Della Ceca R., et al., 2000, in “Large Scale Structure in the X-ray Universe”, Eds. Plionis M. & Georgantopoulos I., Santorini, Greece, September 1999 (astro-ph/0001119)
- Schechter P., 1976, ApJ 203, 297
- Scodeggio M., Olsen L.F., da Costa L., et al., 1999, A&A 137, 83
- Smail I., Dickinson M., 1995, ApJ 455, L99
- Stanford S.A., Eisenhardt P.R., Dickinson M., 1998, ApJ 492, 461
- Tonry J., Davis M., 1979, AJ 84, 1511
- White S.D.M., Efstathiou G., Frenk C.S., 1993, MNRAS 252, 1023
- Zaritsky D., Nelson A.E., Dalcanton J.J., Gonzalez H., 1997, ApJ 480, L91

This figure "eis_efosc2.f1.gif" is available in "gif" format from:

<http://arxiv.org/ps/astro-ph/0005536v1>

This figure "eis_efosc2.f2.gif" is available in "gif" format from:

<http://arxiv.org/ps/astro-ph/0005536v1>

This figure "eis_efosc2.f3.gif" is available in "gif" format from:

<http://arxiv.org/ps/astro-ph/0005536v1>

This figure "eis_efosc2.f4.gif" is available in "gif" format from:

<http://arxiv.org/ps/astro-ph/0005536v1>

This figure "eis_efosc2.f5.gif" is available in "gif" format from:

<http://arxiv.org/ps/astro-ph/0005536v1>

This figure "eis_efosc2.f6.gif" is available in "gif" format from:

<http://arxiv.org/ps/astro-ph/0005536v1>